Arnaud F. M. Bizard
e-mail: afmb2@cam.ac.uk

Digby D. Symons
e-mail: dds11@cam.ac.uk

Norman A. Fleck
e-mail: naf1@cam.ac.uk

Department of Engineering,
Cambridge University,
Cambridge CB2 1PZ, UK

David Durban
Faculty of Aerospace Engineering,
Technion, Israel Institute of Technology,
Technion City,
Haifa 32000, Israel
e-mail: aer6903@techunix.technion.ac.il

Flow of Damp Powder in a Rotating Impervious Cone

A one dimensional analytical model is developed for the steady state, axisymmetric flow of damp powder within a rotating impervious cone. The powder spins with the cone but migrates up the wall of the cone (along a generator) under centrifugal force. The powder is treated as incompressible and Newtonian viscous, while the shear traction at the interface is taken to be both velocity and pressure dependent. A nonlinear second order ordinary differential equation is established for the mean through-thickness velocity as a function of radius in a spherical coordinate system, and the dominant nondimensional groups are identified. For a wide range of geometries, material parameters, and operating conditions, a midzone exists wherein the flow is insensitive to the choice of inlet and outlet boundary conditions. Within this central zone, the governing differential equation reduces to an algebraic equation with an explicit analytical solution. Furthermore, the bulk viscosity of the damp powder does not enter this solution. Consequently, it is suggested that the rotating impervious cone is a useful geometry to measure the interfacial friction law for the flow of a damp powder past an impervious wall.
[DOI: 10.1115/1.4002581]

1 Introduction

1.1 The Conical Centrifuge for Filtration. Centrifugal filters are commonly used in the food processing and chemical industries in order to separate the liquid and solid phases of a mixture, where the two phases have comparable densities. There exist two main types of centrifugal filter: *batch* machines with a cylindrical basket and *continuous* machines with a conical basket. The present study is a first step in analyzing continuous flow within a conical centrifuge, as sketched in Fig. 1.

A typical application of the conical centrifuge is the separation of liquid molasses from sugar crystals in the sugar industry. The rotating basket of the machine spins at about 1000 rpm and comprises a cone with a jump in cone angle along its length: A lower impervious cone has a semiangle of $\alpha=15$ deg, whereas the upper perforated cone has $\alpha=30$ deg (see Fig. 1). The outlet diameter at the top of the upper cone is on the order of 1 m. The inside wall of the upper perforated cone is fitted with a slotted screen, thereby allowing for fluid drainage but preventing powder drainage. The feedstock, in the form of a sugar/molasses slurry, of a liquid volume fraction of 50% and a temperature of 60°C is introduced along the spin axis into the lower impervious cone at a constant flow rate. The slurry acquires the angular velocity of the basket and migrates up the wall of the lower cone into the upper perforated cone. The transition point is labeled station A in Fig. 1. Liquid drainage is rapid within the upper cone, and the slurry evolves into the state of a damp powder (station B in Fig. 1) within the lower 20% of the perforated cone. In the remaining upper 80% of the perforated cone, the liquid volume fraction reduces from 30% to the outlet value of 0.5% (at station C). The microstructure of the solid/liquid/air mixture is shown in Fig. 2 at stations A, B, and C.

In a typical sugar centrifuge, the mass flow rate of sugar/molasses is 30 tonnes/h (8.3 kg/s), the thickness of the powder layer in the upper perforated cone is approximately 5 mm, and the flow velocity along a generator of the cone is on the order of 0.1 m s^{-1}. This implies a residence time of the powder in the machine of approximately 10 s. In comparison, a batch sugar centrifuge spins at full speed for 1 min, and the greater drainage time leads to a lower final liquid content. Thus, it is desirable to increase the residence time of the powder within the continuous conical centrifuge in order to improve the drying efficiency and to allow for additional operations, such as spray washing. To date, this optimization has been done in a largely heuristic manner, and there is a clear need for a quantitative model of powder flow within the machine.

In the current study, we analyze the flow of damp powder within the upper part of the perforated cone. The liquid content and the degree of liquid drainage are minor in this zone, and so the powder can be treated as a homogeneous single phase medium. A major objective of the analysis is to explore the sensitivity of the powder flow to the choice of friction law between powder and cone wall. In order to justify the friction laws adopted, we first present a brief literature review on the nature of the interfacial friction law for the flow of a damp powder past an impervious wall. The constitutive law for the bulk behavior of a damp powder is then briefly discussed.

1.2 Review of Interfacial Friction Law for Damp Powders. It is anticipated that interfacial friction plays a significant role in determining the velocity of flow in a conical centrifuge, and it is recognized that the governing friction law is sensitive to the volume fraction of liquid phase. We consider, in turn, friction laws for a slurry, wet paste, and damp powder.

1.2.1 Slurry Flow. A slurry comprises a suspension of solid particles in a liquid; for a low particulate loading, it can be treated as a Newtonian viscous fluid [1]. Consequently, for slurry flow past a solid boundary at low Reynolds number, the interfacial shear traction τ is obtained by assuming laminar flow and a no-slip condition at the interface. However, the high volume fraction of solid in a paste or a damp powder makes such an approach inappropriate.

1.2.2 Paste Flow. The flow of pastes (liquid saturated powders) in extruders [2] and in capillaries [3] has been studied extensively. For these pastes, liquid migrates from the bulk to the wall [4], creating a fluid-rich interfacial zone. This leads to a low value of shear traction τ compared with the normal pressure p on the wall; for example, τ/p is in the range 0.006–0.04 in Benbow's

Contributed by the Applied Mechanics Division of ASME for publication in the JOURNAL OF APPLIED MECHANICS. Manuscript received June 25, 2010; final manuscript received September 10, 2010; accepted manuscript posted September 17, 2010; published online December 20, 2010. Editor: Robert M. McMeeking.

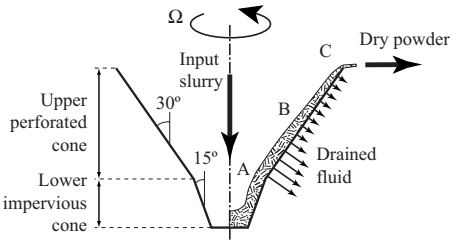

Fig. 1 Cross-section of a typical conical centrifugal filter

experiments on α-alumina [2,5]. Experiments also suggest that the shear traction τ increases linearly with the slip velocity u according to [2]

$$\tau = \tau_0 + au \tag{1}$$

where a is a constant coefficient and τ_0 is the shear strength.

1.2.3 Flow of Damp Powder. Industrial experience and laboratory experiments suggest that the frictional behavior of damp powder differs significantly from that of a paste.

(i) Triaxial tests by Davy et al. [6] on damp sugar revealed that the cohesive strength between particles is negligible; consequently, the shear strength τ_0 at the interface between damp sugar and a centrifuge screen can be neglected.
(ii) Conical centrifuges in the sugar industry have a cone angle of $\alpha = 30$ deg for the flow of damp sugar. It is recognized within the industry [7] that the residence time of the powder is sensitive to the cone angle: If α is too small, the powder sticks to the wall and rapidly accumulates within the machine. Conversely, if α is too large, the powder accelerates out of the basket with a negligible residence time. This suggests that a Coulomb friction law applies at the wall-powder interface such that $\tau/p \approx \tan\alpha = 0.5$. We shall show in the following section that an additional velocity dependence of τ is needed in order to achieve a steady flow within the conical centrifuge.

1.2.4 A One Dimensional Model for Powder Flow in a Conical Centrifuge. Some initial insight is obtained into the problem of damp powder flow within a conical centrifuge by considering the much simplified 1D problem of sliding of a rigid block down an inclined slope under gravity. This classical problem neglects the role of hoop stress and direct straining present within a conical centrifuge, but we shall show later that the 1D problem is an excellent approximation for the practical case of axisymmetric flow.

Consider the sliding of a rigid block of powder of density ρ down a slope of inclination α. For definiteness, assume that the block is a cube of height h. The powder is subjected to a gravitational acceleration g and has a velocity u down the slope at any time t. Assume a friction law of the form

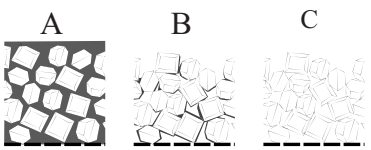

	A	B	C
Solid	50%	60%	60%
Liquid	50%	10%	0.5%
Air	0%	30%	39.5%

Fig. 2 Microstructure and volume fraction of the solid/liquid/air phases at stations A, B, and C

$$\tau = au + bp \tag{2}$$

where b is a constant coefficient of friction and p is the normal pressure on the wall. Upon making use of Eq. (2), the equation of motion reads

$$\rho h\frac{du}{dt} + au = \rho hg\sin\alpha - bp \tag{3}$$

where $p = \rho gh\cos\alpha$. Now, assume that the powder has an initial velocity u_0 at $t=0$. Then, its velocity at time $t \geq 0$ is given by

$$u(t) = u_f + [u_0 - u_f]\exp\left(-\frac{at}{\rho h}\right) \tag{4}$$

where

$$u_f = (1 - b\cot\alpha)\frac{\rho gh}{a}\sin\alpha \tag{5}$$

It is evident from Eq. (4) that u attains a finite final value u_f if $b\cot\alpha$ is less than unity, whereas the block arrests when $b\cot\alpha$ exceeds unity. The value $a=0$ is of special interest as it implies that the shear traction is independent of sliding velocity. For this choice, the solution to Eq. (3) becomes

$$u(t) = u_0 + g\sin\alpha(1 - b\cot\alpha)t \tag{6}$$

with the interpretation that the block speeds up or slows down to arrest, in accordance with the sign of $(1 - b\cot\alpha)$.

This simple model shows that the steady flow of powder down a slope of arbitrary angle (or in a conical centrifuge) demands a velocity-dependent shear traction τ. But what is the physical origin of the velocity dependence for the flow of damp sugar within a conical centrifuge? It is argued that the small amount of drainage of molasses through the powder lubricates the asperities between powder and screen of the basket. The development of a tribological model to describe this is beyond the scope of the present study, and herein, we shall simply use an empirical friction law of type (2). In the present treatment, we assume that the friction law for damp powder past a steel screen has a linear viscous component and a Coulomb friction component as given by Eq. (2) with parameters a and b that depend upon the moisture content of the powder, the screen geometry, and so forth.

1.3 Constitutive Laws for the Bulk Deformation of a Slurry or a Damp Powder. At the inlet to the continuous centrifuge, the slurry feedstock behaves as a Newtonian fluid of dynamic viscosity on the order of 10 Pa s [8]. However, as the liquid phase is drained by centrifugal action, the slurry is reduced to a damp powder. There is some choice in the most appropriate constitutive description for a damp powder [9,10]. We shall show that the constitutive choice for the powder has only a minor influence upon its flow behavior within a large portion of the conical centrifuge. This justifies a major simplification to the analysis: The damp powder is treated as a Newtonian viscous fluid. Other constitutive choices for the damp powder will be the subject of a subsequent study.

1.4 Outline of Paper. A one dimensional analysis is now given for the steady state flow of a damp powder within a conical centrifuge. The analysis assumes that the flow is thin (i.e., that the thickness of the powder layer is much less than the radius of the basket) and that both the gravitational and Coriolis components of acceleration are negligible compared with the centrifugal action. These assumptions match the conditions observed in the practical case of a conical centrifuge as used in the sugar industry. Equilibrium and kinematic relations are established, and a linear viscous constitutive law is adopted for the damp powder. Two choices of friction law are used: (a) a linear viscous law with zero slip at the interface and (b) a pressure and slip-rate dependent law. In each case, a nonlinear ordinary differential equation (ODE) is devel-

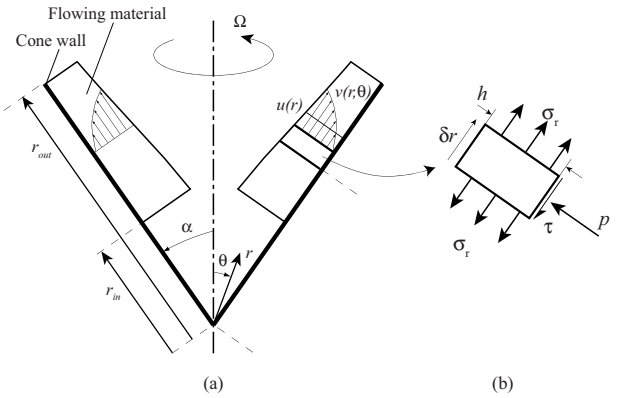

Fig. 3 (*a*) Cone geometry and (*b*) element of material of thickness *h* and of infinitesimal radial thickness *δr*

oped for the thickness averaged flow velocity as a function of radius, and numerical solutions are obtained. In the case of a vanishingly thin (*slender*) flow, the ODE reduces to an algebraic solution for the velocity. The velocity of a flow of small but finite thickness will converge to the slender flow solution in a midzone, which is independent of the inlet and outlet boundary conditions. The size of centrifuge necessary for this midzone to exist is assessed for both choices of friction law.

2 Problem Statement

Consider the steady state laminar flow of a thin fluid layer within a spinning cone of apex angle 2α and constant spin speed Ω, as shown in Fig. 3. Introduce the spherical coordinates (r,θ,ϕ) in a Eulerian reference frame and assume that the fluid has the same circumferential speed (in the ϕ-direction) as the cone at any radius r, as observed in the practical operation of a conical centrifuge. Ω is sufficiently large for the acceleration due to gravity to be negligible compared with $r\Omega^2 \sin\alpha$ at any radius r. Write $v(r,\theta)$ as the radial component of the fluid velocity. We shall simplify the problem by introducing $u(r)$ as the mean value of $v(r,\theta)$ over the thickness $h(r)$ of the thin layer, where the radial velocity $u(r)$ is much less than the circumferential velocity $r\Omega \sin\alpha$ for any radius r. Likewise, the Cauchy stress on a fluid element averaged over its thickness has components $(\sigma_r,\sigma_\theta,\sigma_\phi,\tau_{r\theta})$, which depend only upon r. The wall traction in the r-direction has a normal component $p(r)$ and a shear component $\tau(r)$.

The fluid is treated as incompressible and Newtonian with a density ρ and dynamic viscosity μ. Then, the velocity strain rate tensor $\mathbf{D}$ is related to the deviatoric stress tensor by $\mathbf{S}=2\mu\mathbf{D}$. The fluid enters the cone at the inlet radius r_{in} with a mass flow rate $\dot{m}$ and exits at the outlet radius r_{out}, as shown in Fig. 3(*a*).

The objective is to solve for $u(r)$, assuming two friction laws in turn: Friction law A is a no-slip, linear viscous condition, and friction law B is both pressure and slip-rate dependent. These two choices encompass a wide range of behaviors and include the friction laws commonly used to describe the interface condition for a Newtonian fluid and for a paste as discussed above.

2.1 Friction Law A. No-slip is assumed at the interface, and the fluid is treated as Newtonian viscous. Consequently, a parabolic velocity distribution exists across the thickness of the layer, and the shear traction τ at the interface is dictated by the local velocity gradient, giving

$$\tau = 3\mu\frac{u}{h} \tag{7}$$

2.2 Friction Law B. Alternatively, we consider the flow of a damp powder with velocity and pressure dependent friction at the interface. The fluid velocity is taken to have a slip component u and an additional parabolic component whose average magnitude is $\tilde{u}$ over the thickness of the layer, where $\tilde{u}$ is assumed to be small compared with u. Consequently, the frictional traction is specified by Eq. (2). The interface parameters a and b are taken to be constant over the cone. In the limit $a\to 0$, relation (2) reverts to the familiar Coulomb law with friction coefficient b. The powder bulk is treated as a Newtonian viscous fluid and the basal shear stress can therefore also be written as

$$\tau = 3\mu\frac{\tilde{u}}{h} \tag{8}$$

3 Governing Field Equations

Consider force equilibrium of a thin element of thickness h, as shown in Fig. 3(*b*). Then, equilibrium in the θ-direction gives

$$rp - \frac{1}{r}\frac{d}{dr}(r^2 h\tau_{r\theta}) + h\sigma_\phi \cot\alpha = \Omega^2\rho h r^2 \cos\alpha \sin\alpha \tag{9}$$

while equilibrium in the radial direction provides

$$\frac{d(hr\sigma_r)}{dr} - h(\sigma_\phi + \sigma_\theta) - r\tau = -\rho h r^2\Omega^2 \sin^2\alpha \tag{10}$$

σ_r, σ_θ, σ_ϕ, and $\tau_{r\theta}$ are the average stresses over the thickness of the layer whereas (p,τ) are the normal and shear components of the basal traction. Upon assuming a linear variation of the internal stresses over the thickness, we obtain

$$\sigma_\theta = -\frac{p}{2} \quad \text{and} \quad \tau_{r\theta} = -\frac{\tau}{2} \tag{11}$$

The mass flow rate $\dot{m}$ is independent of r in steady state and is given by

$$\dot{m} = 2\pi r\rho h u \sin\alpha \tag{12}$$

The velocity strain rate tensor $\mathbf{D}$ has the following nonvanishing direct strain components for $\tilde{u} \ll u$:

$$D_r = \frac{du}{dr}, \quad D_\phi = \frac{u}{r}, \quad D_\theta = \frac{u}{h}\frac{dh}{dr} \tag{13}$$

and incompressibility dictates that

$$D_r + D_\phi + D_\theta = 0 \tag{14}$$

4 Friction Model A: Newtonian Flow

A nonlinear second order ODE for $u(r)$ is now derived for friction law A, as specified by Eq. (7). We shall rewrite this ODE in nondimensional form, and to do so, we first introduce a reference solution by considering the slender flow limit. Boundary conditions are stipulated at the inlet and outlet and are used to obtain a numerical solution to the governing nondimensional ODE. A typical solution is reported, and the sensitivity of solution to the independent nondimensional groups is determined.

4.1 A Limiting Case: Slender Flow. Consider the limit of a vanishingly thin flow, where $h/r\to 0$. Then, relations (7), (10), and (12) combine into an algebraic relation for u,

$$u = \left(\frac{\dot{m}^2\Omega^2}{12\pi^2\rho\mu r}\right)^{1/3} \tag{15}$$

At inlet $r=r_{\text{in}}$, the inlet velocity follows immediately as

$$u_A \equiv \left(\frac{\dot{m}^2\Omega^2}{12\pi^2\rho\mu r_{\text{in}}}\right)^{1/3} \tag{16}$$

and the flow velocity $u(r)$ can then be re-expressed as

$$u = u_A \left(\frac{r}{r_{\text{in}}} \right)^{-1/3} \tag{17}$$

The layer thickness at inlet h_A follows from mass conservation (Eq. (12)) as

$$h_A \equiv \frac{\dot{m}}{2\pi\rho r_{\text{in}} u_A \sin\alpha} \tag{18}$$

The equilibrium statement (Eq. (9)) also simplifies in the slender flow limit $h/r \to 0$ to give

$$p = \rho h r \Omega^2 \sin\alpha \cos\alpha \tag{19}$$

with the inlet value

$$p_A \equiv \rho h_A r_{\text{in}} \Omega^2 \sin\alpha \cos\alpha \tag{20}$$

and use of Eqs. (12) and (18) allows us to write

$$\frac{p}{p_A} = \left(\frac{r}{r_{\text{in}}} \right)^{1/3} \tag{21}$$

Likewise, the equilibrium statement (Eq. (10)) reduces to

$$\frac{\tau}{p_A} = \left(\frac{r}{r_{\text{in}}} \right)^{1/3} \tan\alpha \tag{22}$$

The physical interpretation of Eqs. (21) and (22) is clear: Each material element is subjected to an acceleration of $g^* = r\Omega^2 \sin\alpha$, and each element thereby exerts a traction of magnitude $\rho g^* h = p_A (\cos\alpha)^{-1} (r/r_{\text{in}})^{1/3}$ upon the wall with no contribution from the hoop stress. This traction can be resolved into a normal component p and a shear component τ, giving Eqs. (21) and (22), respectively.

4.2 Dimensionless Governing ODE for Friction Law A. It is beneficial to nondimensionalize the above analysis in order to minimize the number of independent variables. In order to obtain the governing equation in nondimensional form, we make use of the reference values u_A, h_A, and p_A defined at the inlet for slender flow to define the following nondimensional groups:

(i) the radial coordinate

$$R \equiv \frac{r}{r_{\text{in}}} \tag{23}$$

(ii) the radius of the cone at exit

$$R_{\text{out}} \equiv \frac{r_{\text{out}}}{r_{\text{in}}} \tag{24}$$

(iii) the velocity

$$U \equiv \frac{u}{u_A} \tag{25}$$

(iv) a Reynolds number for friction law A is introduced in terms of u_A and h_A as

$$P_A \equiv \frac{\dot{m}}{\mu r_{\text{in}} \sin\alpha} = \frac{2\pi\rho u_A h_A}{\mu} \tag{26}$$

(v) the slenderness ratio of layer thickness to radius is defined as

$$Q_A \equiv \frac{h_A \cot\alpha}{r_{\text{in}}} = \frac{\dot{m} \cot\alpha}{2\pi\rho r_{\text{in}}^2 u_A \sin\alpha} \tag{27}$$

The relevant Rossby number in the present problem is

$$\text{Ro} \equiv \frac{u_A}{r_{\text{in}} \Omega \sin\alpha} \tag{28}$$

following Makarytchev et al. [11]. Use of Eqs. (26) and (27) immediately gives

$$\text{Ro} = \left(\frac{P_A Q_A}{6\pi \cot\alpha} \right)^{1/2} \tag{29}$$

A Rossby number of much less than unity implies that the Coriolis acceleration is much less than the centrifugal acceleration. For practical centrifuges, P_A and Q_A are each much less than unity, and so Eq. (29) implies $\text{Ro} \ll 1$, consistent with our initial assumptions.

We proceed to obtain the governing ODE in nondimensional form. Upon introducing the notation

$$(\,)' = \frac{d}{dR} = r_{\text{in}} \frac{d}{dr} \tag{30}$$

and making use of the above normalizations, Eq. (10) can be re-expressed as a governing ODE in $U(R)$ as follows. Express the hydrostatic stress $\sigma_h = (\sigma_r + \sigma_\phi + \sigma_\theta)/3$ in terms of r, u, and du/dr by eliminating p, h, and σ_ϕ from Eq. (9) via Eqs. (11)–(14). Equation (10) can then be re-expressed as

$$A_1 U'' + A_2 \frac{U'^2}{U} + A_3 \frac{U'}{R} + A_4 \frac{U}{R^2} = 0 \tag{31}$$

where the nondimensional coefficients $A_{i(i=1,2,3,4)}$ read

$$A_1 \equiv \xi_1^2 (38 - 27\xi_1 + 4\xi_1^2) \tag{32}$$

$$A_2 \equiv -2\xi_1^2 (19 - 8\xi_1 + 2\xi_1^2) \tag{33}$$

$$A_3 \equiv \frac{24\xi_1 \cot\alpha^2}{RU^3} + 2\xi_1^2 \frac{(-14RU^3 - 3\cot\alpha^2)}{RU^3} - 38\xi_1^3 + 4\xi_1^4 \tag{34}$$

$$A_4 \equiv \frac{24(1 - RU^3)\cot\alpha^2}{RU^3} + 24\xi_1 \cot^2\alpha - 6\xi_1^2 \left[14 - \frac{(1 - RU^3)\cot^2\alpha}{RU^3} \right] - 26\xi_1^3 + 12\xi_1^4 \tag{35}$$

where

$$\xi_1 \equiv \frac{Q_A}{R^2 U} \tag{36}$$

Note that the coefficients A_i depend upon (R, U) in a nonlinear manner but are independent of the derivatives of $U(R)$.

4.2.1 The Slender Flow Limit in Nondimensional Form. In the limit of the slender flow ($h/r \to 0$ or, equivalently, $Q_A \to 0$ according to Eq. (27)), Eq. (31) reduces to Eq. (17), and this can be rewritten as

$$U = \bar{U} \equiv R^{-1/3} \tag{37}$$

Likewise, Eqs. (21) and (22) and the mean and direct deviatoric components of stress in a slender flow reduce to

$$\frac{p}{p_A} = R^{1/3} \tag{38}$$

$$\frac{\tau}{p_A} = R^{1/3} \tan\alpha \tag{39}$$

$$\frac{\sigma_h}{p_A} = -\frac{R^{1/3}}{2} \tag{40}$$

$$\frac{S_r}{p_A} = \frac{-2Q_A \tan^2\alpha}{9R^{4/3}} \tag{41}$$

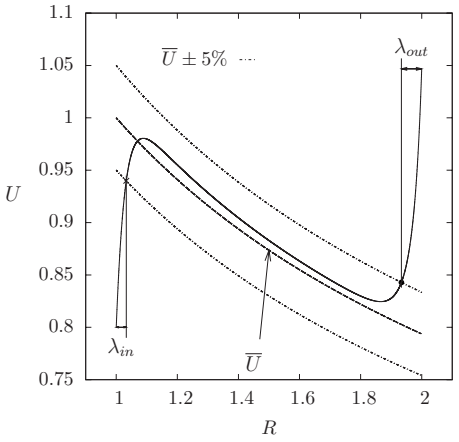

Fig. 4 Friction law A: solution compared with $\bar{U}$ for $\alpha = 30$ deg and $Q_A = 0.1$

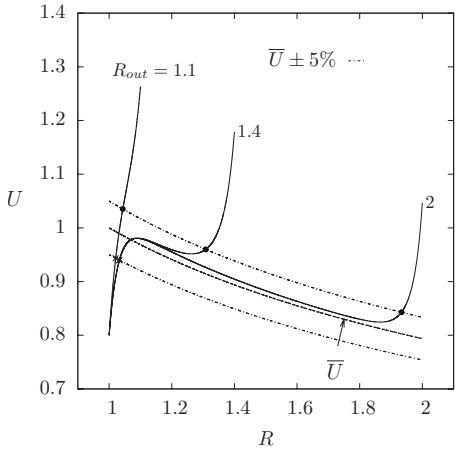

Fig. 5 Friction law A: solutions for various values of R_{out} compared with $\bar{U}$ with $\alpha = 30$ deg and $Q_A = 0.1$

$$\frac{S_\phi}{p_A} = \frac{2Q_A \tan^2 \alpha}{3R^{4/3}} \tag{42}$$

$$\frac{S_\theta}{p_A} = \frac{-4Q_A \tan^2 \alpha}{9R^{4/3}} \tag{43}$$

It is clear from Eqs. (38)–(43) that the hydrostatic stress σ_h and the wall traction (p, τ) greatly exceed the direct components of the deviatoric stress tensor (S_r, S_ϕ, S_θ) in a slender flow.

4.3 Numerical Solution of the Governing ODE

4.3.1 The Boundary Conditions. At the inlet to the perforated cone of a conical centrifuge for sugar refinement, there exists a jump in cone angle from $\alpha = 15$ deg to $\alpha = 30$ deg. Consequently, the inlet velocity for the perforated cone is set by the slender flow solution that has already been established within the lower imperforate cone. This implies an inlet value of U on the order of

$$U = 0.8 \quad \text{at} \quad R = 1 \tag{44}$$

At the outlet, the interfacial pressure vanishes, and we model this as $p(r_{\text{out}}) = 0$. This leads to the following relation between the outlet velocity U_{out} and its first derivative U'_{out}:

$$U'_{\text{out}} = \frac{6R_{\text{out}}^3 \cot^2 \alpha - 14R_{\text{out}}^2 U_{\text{out}}^2 Q_A - 4U_{\text{out}} Q_A^2}{19R_{\text{out}}^3 U_{\text{out}} Q_A - 4R_{\text{out}} Q_A^2} \tag{45}$$

upon making use of Eqs. (9), (13), and (23)–(30). We shall show below that the flow over most of the cone is insensitive to the choice of boundary conditions, provided that R_{out} is sufficiently large.

The dimensionless ODE (Eq. (31)) has been solved numerically using the algorithm *bvp5c* of MATLAB [12]. A typical solution for $U(R)$ is given in Fig. 4 for $\alpha = 30$ deg, $P_A = 1$, and $Q_A = 0.1$. The boundary conditions are specified by Eqs. (44) and (45). The slender flow solution $\bar{U}(R)$ is included in Fig. 4 and lies close to $U(R)$ except at the inlet and outlet. $U(R)$ lies within 5% of $\bar{U}$ at a distance λ_{in} from the inlet and at a distance λ_{out} from the outlet. We interpret λ_{in} and λ_{out} as the lengths of the inlet and outlet transition regions, respectively.

4.3.2 Cross-Coupling of the Inlet and Outlet Boundary Conditions: The Limiting Cone Size $R_{\text{out}}^{\text{lim}}$. Solutions of the ODE (Eq. (31)) are given in Fig. 5 for selected values of R_{out} and for the specific values $\alpha = 30$ deg, $P_A = 1$, and $Q_A = 0.1$. Write $R_{\text{out}}^{\text{lim}}$ as the limiting value of R_{out} for which $U(R)$ lies within 5% of $\bar{U}$ over a portion of 80% of the cone.

It remains to explore the sensitivity of $R_{\text{out}}^{\text{lim}}$ to α, P_A, and Q_A. Within the range of validity of the model, $R_{\text{out}}^{\text{lim}}$ is insensitive to the magnitude of P_A. The dependence of $R_{\text{out}}^{\text{lim}}$ upon α and Q_A is plotted as a map in Fig. 6. An example working point is marked as a cross on this map based upon the following values representative of a typical sugar centrifuge:

$$\alpha = 30 \text{ deg}, \quad \dot{m} = 8.3 \text{ kg s}^{-1}, \quad \Omega = 1000 \text{ rpm}$$

$$r_{\text{in}} = 0.54 \text{ m}, \quad r_{\text{out}} = 1.185 \text{ m}, \quad \rho = 1.4 \text{ Mg m}^{-3}, \quad \mu = 10 \text{ Pa s} \tag{46}$$

These lead to $u_A = 0.94$ m s^{-1}, $P_A = 3.1$, $Q_A = 1.2 \times 10^{-2}$, $R_{\text{out}} = 2.2$ and $R_{\text{out}}^{\text{lim}} = 1.10$. Since R_{out} is significantly larger than $R_{\text{out}}^{\text{lim}}$, the flow behavior over much of the cone is given by the slender flow result (Eq. (37)).

It is clear from Fig. 6 that over a wide range of values for Q_A and for α, the value of $R_{\text{out}}^{\text{lim}}$ is less than 1.5. Practical centrifuges possess a value for R_{out} greater than this and so a central region of slender flow is predicted.

4.3.3 Dominant Dimensionless Groups for the Flow Behavior. Numerical experimentation has been performed to determine the change in limit radius $\Delta R_{\text{out}}^{\text{lim}}$ due to changes in cone angle $\Delta\alpha$, in slenderness ratio ΔQ_A, and in Reynolds number ΔP_A for the operating point, as specified in Eq. (46). The first order sensitivity reads

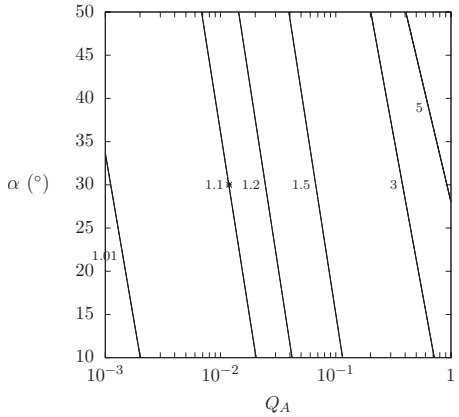

Fig. 6 Friction law A: contours of $R_{\text{out}}^{\text{lim}}$ in the (α, Q_A) plane, the star marks the working point of a typical low-grade sugar continuous centrifuge

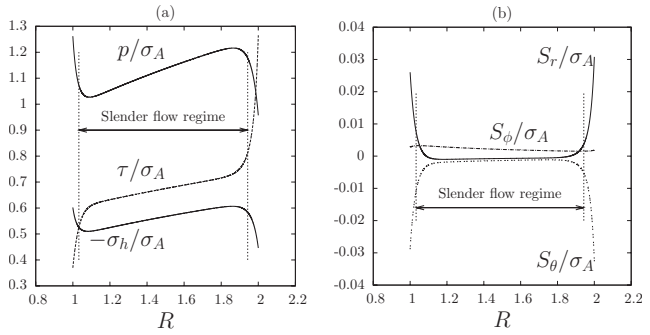

Fig. 7 Friction law A: dimensionless stresses for α=30 deg, Q_A=0.1, and R_{out}=2. (*a*) Hydrostatic stress σ_h and wall traction (τ, p) and (*b*) direct components of the deviatoric stress tensor.

$$\frac{\Delta R_{out}^{lim}}{R_{out}^{lim}} = 0.055\frac{\Delta\alpha}{\alpha} + 0.037\frac{\Delta Q_A}{Q_A} \tag{47}$$

P_A does not have any influence on R_{out}^{lim} as it does not appear in Eq. (31) since the convective terms have been neglected in Eq. (10).

4.3.4 The Stress State Within the Flow. It is instructive to plot the traction distribution and the stress distribution throughout the flow. The through-thickness averaged stresses are plotted in Fig. 7 for the case already reported in Fig. 4 with α=30 deg, Q_A=0.1, and R_{out}=2.

Recall that in the central portion of the cone (away from inlet and outlet), the flow is adequately approximated by the slender flow solution (Eq. (37)). Likewise, the stress state in the central portion is well represented by Eqs. (38)–(43), although the asymptotic analysis is not shown in Fig. 7 as it would clutter the figure. Throughout the flow, the hydrostatic stress is compressive and dominates the direct deviatoric stresses (S_r, S_ϕ, and S_θ), and consequently, the stress components σ_r, σ_θ, and σ_ϕ are compressive. Thus, there is no tendency for the powder flow to develop radial fissures.

5 Friction Model B: Coulomb Friction With Slip-Rate Dependence

A nonlinear second order ODE for $u(r)$ is now derived for friction law B of specification (2). In a similar fashion to that outlined for friction law A, we introduce a reference solution by considering the slender flow limit, and we then use this reference solution to write the governing ODE in nondimensional form. The same boundary conditions as those used in model A are enforced. A typical solution is reported, and the sensitivity of solution to the independent nondimensional groups is determined.

5.1 The Slender Flow Case. Consider the limit $h/r \to 0$. Equations (2), (10), and (12) combine into an algebraic relation for u

$$u = u_B \equiv \left(\frac{(1 - b\cot\alpha)\dot{m}\Omega^2 \sin\alpha}{2\pi a}\right)^{1/2} \tag{48}$$

Note that the expression (48) for u is independent of r in contrast to the result (Eq. (17)) for friction law A. The layer thickness at inlet h_B follows from mass conservation (Eq. (12)) as

$$h_B \equiv \frac{\dot{m}}{2\pi\rho r_{in} u_B \sin\alpha} \tag{49}$$

In similar fashion to that outlined for model A, the equilibrium relation in the θ-direction (Eq. (9)) reduces to Eq. (19), and at inlet, this gives

$$p_B \equiv \rho h_B r_{in}\Omega^2 \sin\alpha\cos\alpha \tag{50}$$

For any radius r, the equilibrium (Eqs. (9) and (10)) reduces to

$$p/p_B = 1 \tag{51}$$

$$\tau/p_B = \tan\alpha \tag{52}$$

The physical interpretation of Eqs. (51) and (52) is identical to that given for friction law A: The wall traction derives solely from the centrifugal weight of the powder. Note that the bulk constitutive law for the powder does not enter Eqs. (48)–(52).

Upon making use of Eqs. (2), (8), and (52), $\tilde{u}$ can be related to the slip velocity u via

$$\tilde{u} = \frac{ahu}{3\mu(1 - b\cot\alpha)} \tag{53}$$

Consequently, the through-thickness averaged shear stress $\tau_{r\theta}$ can be obtained via Eqs. (8) and (11) as

$$\tau_{r\theta} = -\tfrac{1}{2}\frac{au}{(1 - b\cot\alpha)} \tag{54}$$

(As already mentioned, we shall restrict attention to the practical case $\tilde{u} \ll u$.)

5.2 The Dimensionless Problem. Upon making use of the reference values u_B, h_B, and p_B defined at the inlet for the slender flow, the governing equation for model B is obtained in dimensionless form by introduction of the following nondimensional groups.

(i) The dimensionless velocity U is

$$U \equiv \frac{u}{u_B} \tag{55}$$

(ii) A Reynolds number is introduced as

$$P_B \equiv \frac{\rho u_B}{a} \tag{56}$$

(iii) A slenderness aspect ratio of layer thickness to radius is taken as

$$Q_B \equiv \frac{h_B}{r_{in}}\cot\alpha = \frac{\dot{m}\cot\alpha}{2\pi\rho r_{in}^2 u_B \sin\alpha} \tag{57}$$

Attention is restricted to the thin flow case $Q_B < 0.1$.

(iv) The dimensionless coefficient for rate-dependent friction reads

$$\hat{\mu} \equiv \frac{ah_B}{\mu} \tag{58}$$

(v) The ratio of friction angle to cone angle is expressed in terms of the parameter

$$\hat{b} \equiv b\cot\alpha \tag{59}$$

Note that the ratio of $\tilde{u}$ to u (Eq. (53)) can be re-expressed in terms of the dimensionless parameters as

$$\frac{\tilde{u}}{u} = \frac{\hat{\mu}}{3(1 - \hat{b})RU} \tag{60}$$

It has already been assumed that $\tilde{u}$ is small compared with u. Given that a typical friction ratio for a conical centrifuge is $\hat{b} \approx 0.9$, an upper limit for this model to be valid is therefore given by $\hat{\mu} < 0.1$. The Rossby number at the inlet is

$$\mathrm{Ro} \equiv \frac{u_B}{r_{in}\Omega \sin\alpha} = ((1 - \hat{b})P_B Q_B \tan\alpha)^{1/2} \tag{61}$$

In practical centrifuges, P_B and Q_B are both much less than unity, while $\hat{b}$ is nearly unity, implying that Ro is much less than unity, so that centrifugal forces dominate and are consistent with the model assumptions. In the general case

of a thin flow, the nondimensional flow velocity U is a function of R, α, $\hat{b}$, $\hat{\mu}$, P_B, and Q_B. The procedure to obtain the governing ODE follows that outlined for friction law A, but now, τ is eliminated via Eq. (2) and $\tau_{r\theta}$ via Eq. (54). The resulting ODE reads

$$B_1 U'' + B_2 \frac{U'^2}{U} + B_3 \frac{U'}{R} + B_4 \frac{U}{R^2} = 0 \tag{62}$$

where the nondimensional coefficients (B_1, B_2, B_3, B_4) read

$$B_1 = (8 - 6\xi_1 + \xi_1^2)\xi_2 \tag{63}$$

$$B_2 = -(8 - 4\xi_1 + \xi_1^2)\xi_2 \tag{64}$$

$$B_3 = -4\xi_2(1-\hat{b}) - 2\xi_1(-1 + (4+\hat{b})\xi_2) + \frac{\xi_1^2(-1 + 2\xi_2 - U^2 \tan^2 \alpha)}{2} \tag{65}$$

$$B_4 = 2(1-\hat{b})(1-U^2) + 4(-3+2\hat{b})\xi_2 + \xi_1(\hat{b} + 2(1-\hat{b})U^2 - 4(2+\hat{b})\xi_2 + \hat{b}U^2 \tan^2 \alpha) + \frac{-(\xi_1^2(-1 + U^2 - \hat{b}U^2 - 6\xi_2 + (4+\hat{b})U^2 \tan^2 \alpha))}{2} + \frac{U^2 \xi_1^3 \tan^2 \alpha}{2} \tag{66}$$

in terms of

$$\xi_1 \equiv \frac{h \cot \alpha}{r} = \frac{Q_B}{R^2 U} \tag{67}$$

$$\xi_2 \equiv \frac{Q_B^2 U(1-\hat{b})\tan^2 \alpha}{\hat{\mu} R^3} \tag{68}$$

We emphasize that Eq. (62) is the governing second order nonlinear ODE for $U(R)$ with nonconstant coefficients dependent upon R and U in addition to the four constant dimensionless groups $(Q_B, \hat{\mu}, \hat{b}, \alpha)$. The Reynolds number P_B does not enter Eq. (62).

5.2.1 The Slender Flow Case in Nondimensional Form. For the limiting case of a slender layer, Eq. (48) can be rewritten in a nondimensional notation as

$$U = 1 \tag{69}$$

We note that $Q_B \to 0$ in Eq. (62) leads to the same result. The stress components simplify to

$$p/p_B = 1 \tag{70}$$

$$\tau/p_B = \tan \alpha \tag{71}$$

$$\sigma_h/p_B = -\tfrac{1}{2} \tag{72}$$

$$S_r/p_B = 0 \tag{73}$$

$$S_\phi/p_B = \frac{2Q_B \tan^2 \alpha(1-\hat{b})}{\hat{\mu} R} \tag{74}$$

$$S_\theta/p_B = -\frac{2Q_B \tan^2 \alpha(1-\hat{b})}{\hat{\mu} R} \tag{75}$$

5.3 Numerical Solution of the Governing ODE

5.3.1 The Boundary Conditions. The same boundary conditions as for friction law A are employed: $U=0.8$ at entry and $\sigma_r = 0$ at exit. The outlet boundary condition can now be re-expressed as

$$U'_{\text{out}} = -\frac{Q_B(-2(1-\hat{b})Q_B - \hat{\mu}\pi R_{\text{out}})U_{\text{out}}}{2(1-\hat{b})Q_B R_{\text{out}}(Q_B - 8\pi R_{\text{out}}^2 U_{\text{out}})} - \frac{2\pi R_{\text{out}}^2(\hat{\mu}\pi R_{\text{out}} - 2(1-\hat{b})Q_B U_{\text{out}}^2 + (\hat{\mu}\pi R_{\text{out}} + 2(1-\hat{b})Q_B U_{\text{out}}^2)\cos 2\alpha)\csc^2 \alpha}{2(1-\hat{b})Q_B R_{\text{out}}(Q_B - 8\pi R_{\text{out}}^2 U_{\text{out}})} \tag{76}$$

upon making use of Eqs. (9), (11), (13), and (55)–(59).

5.3.2 A Typical Solution. The algorithm *bvp5c* of MATLAB [12] is used to solve the governing ODE (Eq. (62)), in a similar manner to that used for solving Eq. (31). A typical solution is given in Fig. 8. The values (Eq. (46)) are again used to represent a continuous conical centrifuge in the sugar industry, but now the value $\mu = 10$ Pa s in model A is replaced by the values

$$\mu = 10\,000 \text{ Pa s}, \quad a = 10 \text{ kPa s m}^{-1}, \quad b = 0.5 \tag{77}$$

in friction model B. Here, a has been estimated using the results of Ref. [13], assuming a lubricant dynamic viscosity of 1 Pa s and a mean particle size of 0.5 mm. The bulk viscosity μ has been estimated from the results of shear box tests: μ is given as the shear stress divided by the shear rate. These give $u_B = 0.31$ m s^{-1}, $P_B = 4.4 \times 10^{-2}$, $Q_B = 3.6 \times 10^{-2}$, $\hat{\mu} = 1.1 \times 10^{-2}$, $\hat{b} = 0.87$, and $R_{\text{out}} = 2.2$. The velocity U increases with R from the prescribed inlet value of $U=0.8$ and attains the value $U=1$ for a slender flow over a central region. Then, near exit, the flow deviates from the slender flow solution and U increases sharply with R

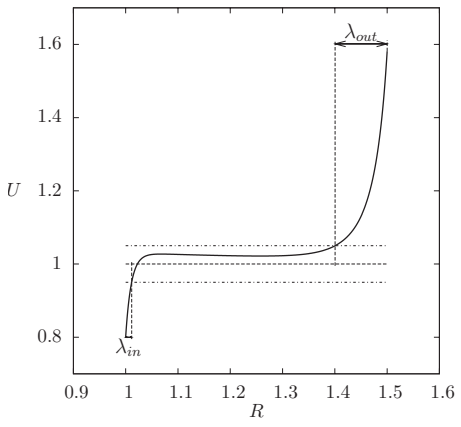

Fig. 8 Model B: ODE solution for α=30 deg, $\hat{b}$=0.9, $\hat{\mu}$=10^{-1}, Q_B=10^{-2}, and R_{out}=1.5

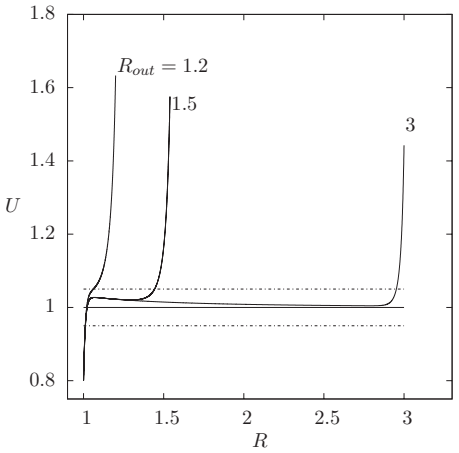

Fig. 9 Model B: ODE solutions for various values of R_{out} with α=30 deg, $\hat{b}$=0.9, $\hat{\mu}=10^{-1}$, and $Q_B=10^{-2}$

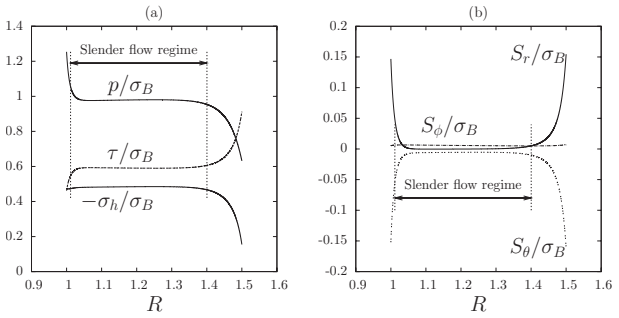

Fig. 11 Model B nondimensionalized stresses: (*a*) hydrostatic stress σ_h and wall traction (τ, p) (*b*) direct components of the deviatoric stress tensor, α=30 deg, $\hat{b}$=0.9, $\hat{\mu}=10^{-1}$, $Q_B=10^{-2}$, and R_{out}=1.5

in order to satisfy Eq. (76) at exit. The transition lengths at the inlet and exit, λ_{in} and λ_{out}, respectively, are defined in the same manner as for model A: Within the transition zones, U deviates from the slender flow result $U=1$ by more than 5%.

5.3.3 Coupling of the Boundary Conditions: The Limit Cone Size R_{out}^{lim}. Solutions to Eq. (62) for $U(R)$ are given in Fig. 9 for a selection of values of R_{out}, but with α, $\hat{b}$, $\hat{\mu}$, P_B, and Q_B held fixed at the values used for constructing Fig. 8. In a similar manner to that noted for model A, the boundary conditions are decoupled when R_{out} exceeds R_{out}^{lim}, defined as the cone size below which the velocity lies within less than 5% of the slender flow solution for less than 80% of the cone.

5.3.4 Dominant Dimensionless Groups for Flow Behavior. The sensitivity of R_{out}^{lim} to the four dominant nondimensional groups is plotted as a map in the α and Q_B and $\hat{b}$ and $\hat{\mu}$ planes in Figs. 10(*a*) and 10(*b*), respectively, for the choice of parameters used in constructing Fig. 8.

The sensitivity of R_{out}^{lim} to the dimensionless independent parameters is now investigated. Numerical experimentation has been performed to determine the change in limit radius ΔR_{out}^{lim} due to a change in cone angle $\Delta\alpha$, in slenderness ratio ΔQ_B, in shear coefficient $\Delta\hat{\mu}$, in friction coefficient Δb, and in Reynolds number ΔP_B for the values specified in Eq. (77). The first order sensitivity reads

$$\frac{\Delta R_{out}^{lim}}{R_{out}^{lim}} = 1.2\frac{\Delta\hat{b}}{\hat{b}} + 0.45\frac{\Delta Q_B}{Q_B} + 0.29\frac{\Delta\alpha}{\alpha} - 0.12\frac{\Delta\hat{\mu}}{\hat{\mu}} \tag{78}$$

5.3.5 The Stress State Within the Flow. The traction and stress distribution for the typical case already reported in Fig. 8 are plotted in Fig. 11. The wall traction and the hydrostatic pressure dominate the direct deviatoric stresses (S_r, S_φ, and S_θ) over much of the cone. A similar behavior was noted in Fig. 7 for model A. Again, the through-thickness averaged Cauchy stresses within the material σ_r, σ_θ, and σ_φ are compressive everywhere.

5.4 Slender Flow Solution for a Drucker–Prager Solid. The above analysis assumes that the bulk response is linear viscous: This is appropriate for the case where the liquid content is high [1]. Densely packed dry powders are better represented by granular flow constitutive models such as the Drucker–Prager law [6,9]. The behavior of damp powder is bounded by these two limiting constitutive responses. We consider in the Appendix a dry powder endowed with the Drucker–Prager yield criterion

$$\sigma_e = -\beta\sigma_h, \quad \sigma_h \leq 0 \tag{79}$$

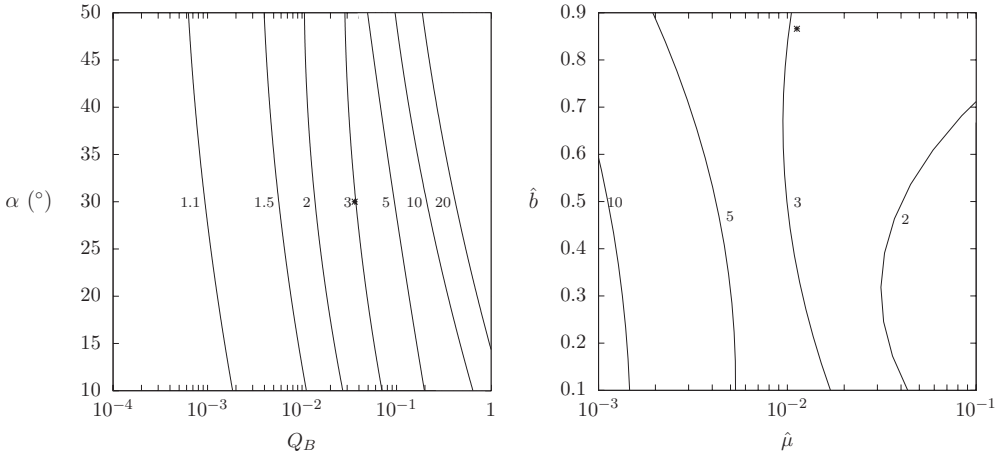

Fig. 10 Model B: Limit radius R_{out}^{lim} linearized contours versus (*a*) Q_B and α and (*b*) $\hat{\mu}$ and $\hat{b}$ with the appropriate parameters held constant at α=30 deg, $\hat{b}$=0.87, $\hat{\mu}=1.1\times10^{-2}$, $P_B=4.4\times10^{-2}$, and $Q_B=3.6\times10^{-2}$. The star on each map marks the working point of a typical low-grade sugar continuous centrifuge.

$$\sigma_e = 0, \quad \sigma_h > 0 \tag{80}$$

where the friction coefficient β is of order unity for sugar crystals [6]. The slender flow solution outlined below has the feature that $\sigma_h < 0$, so that Eq. (79) applies. Incompressible flow is assumed so that the deviatoric stress is codirectional with the strain rate tensor $\mathbf{D}$ with a plastic multiplier λ such that

$$\mathbf{D} = \lambda \mathbf{S} \tag{81}$$

as observed in Ref. [6]. The slender flow regime is derived in the Appendix for this constitutive law for the case of friction model B. Therein, it is shown that the velocity profile $u(r)$ is unchanged from that given by Eq. (48) for a linear viscous bulk flow. Likewise, the wall traction is unchanged and given by Eqs. (51) and (52). The strain rates remain unchanged, but the stress state is modified to

$$\sigma_r = -\frac{p_B}{2}\left(\frac{\sqrt{3}}{\sqrt{3}+\beta}\right) \tag{82}$$

$$\sigma_\phi = -\frac{p_B}{2}\left(\frac{\sqrt{3}-\beta}{\sqrt{3}+\beta}\right) \tag{83}$$

$$\sigma_\theta = -\frac{p_B}{2} \tag{84}$$

$$\tau_{r\theta} = -\frac{p_B \tan\alpha}{2} \tag{85}$$

σ_r and σ_θ are always compressive, and the hoop stress σ_ϕ is compressive, provided $\beta < \sqrt{3}$. For dry sugar, Davy et al. [6] measured β as about 0.7, and so $\sigma_\phi < 0$.

6 Concluding Remarks

This paper provides a first step in the analysis of flow of a wet granular material in a conical centrifugal filter. A one dimensional model of the steady state axisymmetric flow in a spinning impervious cone has been developed. Two different models have been considered for the interfacial shear traction: Model A assumes no-slip laminar Newtonian flow, whereas model B assumes slip with a velocity and pressure dependent shear traction.

For both friction models, the flow is independent of the boundary conditions in a central portion of the cone. Within this zone, the flow velocity is controlled only by the interfacial shear traction and is independent of the bulk stress in the flow (and therefore largely independent of the constitutive model chosen for the bulk behavior). For example, we have shown explicitly that the sliding velocity $u(r)$ in the central portion of the cone is the same for a Drucker–Prager solid as for the linear viscous case. Transition zones exist near the inlet and near the exit. Therein, the flow is sensitive to both the interfacial friction law and to the bulk constitutive law for the powder.

If friction model A is adopted for the interface shear traction, then the length of the transition zones is a function of the cone angle and of the flow thickness but is almost independent of other parameters. However, if model B is adopted, then the Coulomb friction coefficient and the magnitude of the interfacial viscosity relative to the bulk viscosity strongly influence the transition lengths.

The results of this study provide a theoretical framework to extract the friction parameters at the paste/wall interface without dependence upon the paste constitutive relation or the boundary conditions from simple experiments using impervious cones.

Acknowledgment

The authors would like to thank Dr. Clive Grimwood for his technical expertise and are grateful to the Ashby Scholarship Fund and the Cambridge European Trust for financial support.

Nomenclature

- a = slip velocity dependence friction coefficient
- $A_{i,i=1..4}$ = dimensionless, nonconstant coefficients of the governing ODE for model A
- b = Coulomb friction coefficient
- $\hat{b}$ = ratio of Coulomb friction coefficient to cone slope
- $\mathbf{D}$ = velocity strain rate tensor
- D_r = radial strain rate
- D_ϕ = hoop strain rate
- D_θ = through-thickness strain rate
- g = gravitational acceleration
- g^* = local centripetal acceleration within the cone
- h = damp powder thickness normal to the cone surface
- $h_{A,B}$ = reference flow thickness for model A/B
- $\dot{m}$ = mass flow rate
- p = contact pressure at the cone/damp powder interface
- $p_{A,B}$ = reference pressure for model A/B
- $P_{A,B}$ = Reynolds number in the bulk material for model A/B
- $Q_{A,B}$ = flow slenderness ratio for model A/B
- r = radial coordinate measured along the cone's generatrix from the cone's axis
- $r_{\text{in,out}}$ = cone radius at the cone inlet/outlet
- R = dimensionless radial coordinate
- R_{out} = dimensionless outer radial coordinate
- $R_{\text{out}}^{\text{lim}}$ = limit cone radius at outlet for coupling of the boundary conditions
- Ro = Rossby number
- $\mathbf{S}$ = deviatoric stress tensor
- $S_{r,\theta,\phi}$ = deviatoric stress in the radial/through-thickness/hoop direction
- t = time
- u = through-thickness averaged radial flow velocity for model A, slip velocity for model B
- $u_{A,B}$ = reference velocity for model A/B
- u_f = final velocity of the steadily sliding block
- u_0 = initial velocity of the sliding block
- $\bar{u}$ = through-thickness average of the radial parabolic velocity component for model B
- U = dimensionless through-thickness averaged velocity
- U_{out} = exit velocity
- $\bar{U}$ = dimensionless slender flow velocity for model A
- v = local radial flow velocity
- z = coordinate normal to the wall surface
- α = cone half-angle
- β = friction coefficient for the Drucker–Prager solid
- $\Delta R_{\text{out}}^{\text{lim}}$ = change in limit cone radius at outlet due to a change in dimensionless parameters
- λ = plastic multiplier of the Drucker–Prager solid
- $\lambda_{\text{in,out}}$ = convergence length of the governing ODE solution toward the dominant solution at the inlet/outlet
- μ = bulk material dynamic viscosity
- $\hat{\mu}$ = dimensionless lubrication coefficient
- Ω = cone rotational speed
- ρ = bulk material density
- $\sigma_{r,\theta,\phi}$ = cauchy direct stress in the radial/through-thickness/hoop direction
- τ = shear stress at the cone/damp powder interface
- τ_0 = shear strength at the cone/damp powder interface

$\tau_{r\theta}$ = shear stress at mid-depth of the flow
θ = polar angle
ϕ = hoop (azimuthal) angle
ξ_1 = dimensionless nonconstant slenderness ratio
$'$ = differentiation with respect to R

Appendix

The slender flow solution is derived for friction model B and a Drucker–Prager bulk behavior as given by Eq. (79). The rate independent, nonassociated flow case is assumed, as specified by Eq. (81). The assumption of rate independence is supported by the triaxial tests on sugar crystals performed by Davy et al. [6]. In the limit $h/r \to 0$, the equilibrium relations (9) and (10) reduce to the algebraic expressions (48), (51), and (52) for u, τ, and p, respectively. Likewise, the slender flow velocity strain rates reduce to

$$D_r = 0 \tag{A1}$$

$$D_\phi = \frac{u_B}{r} \tag{A2}$$

$$D_\theta = -\frac{u_B}{r} \tag{A3}$$

as for the linear viscous bulk behavior considered in Sec. 5. There is some modification to the stress state, however, from that of the linear viscous behavior. The plastic multiplier λ as defined in Eq. (A4) is obtained from Eqs. (79)–(81) and (A1)–(A3) as

$$\lambda = -\frac{\sqrt{3}u_B}{\beta r \sigma_h} \tag{A4}$$

The deviatoric direct stress components $\mathbf{S}_{ij}$ follow from Eqs. (81) and (A1)–(A4) as

$$\mathbf{S}_r = 0 \tag{A5}$$

$$\mathbf{S}_\phi = -\frac{\beta\sigma_h}{\sqrt{3}} \tag{A6}$$

$$\mathbf{S}_\theta = \frac{\beta\sigma_h}{\sqrt{3}} \tag{A7}$$

and the hydrostatic stress is obtained from Eqs. (11), (51), and (A7) as

$$\sigma_h = \sigma_\theta - \mathbf{S}_\theta = -\frac{p_B}{2}\left(\frac{\sqrt{3}}{\sqrt{3}+\beta}\right) \tag{A8}$$

Upon making use of Eqs. (79)–(81) and (A8), the components of the Cauchy stress tensor at midheight follow immediately as

$$\sigma_r = -\frac{p_B}{2}\left(\frac{\sqrt{3}}{\sqrt{3}+\beta}\right) \tag{A9}$$

$$\sigma_\phi = -\frac{p_B}{2}\left(\frac{\sqrt{3}-\beta}{\sqrt{3}+\beta}\right) \tag{A10}$$

$$\sigma_\theta = -\frac{p_B}{2} \tag{A11}$$

$$\tau_{r\theta} = -\frac{p_B \tan\alpha}{2} \tag{A12}$$

We note that these stress components are of comparable magnitude to p_B, justifying our assumption that Eqs. (9) and (10) reduce to Eqs. (51) and (52) when $h/r \to 0$. Consequently, the slender flow velocity profile is identical to that predicted by the linear viscous result, $u(r) = u_B$.

References

[1] Oliver, D. R., and Ward, S. G., 1953, "Relationship Between Relative Viscosity and Volume Concentration of Stable Suspensions of Spherical Particles," Nature (London), **171**(4348), pp. 396–397.
[2] Benbow, J. J., Oxley, E. W., and Bridgwater, J., 1987, "The Extrusion Mechanics of Pastes—The Influence of Paste Formulation on Extrusion Parameters," Chem. Eng. Sci., **42**(9), pp. 2151–2162.
[3] Yilmazer, U., and Kalyon, D. M., 1989, "Slip Effects in Capillary and Parallel Disk Torsional Flows of Highly Filled Suspensions," J. Rheol., **33**(8), pp. 1197–1212.
[4] Burbidge, A. S., Bridgwater, J., and Saracevic, Z., 1995, "Liquid Migration in Paste Extrusion," Chem. Eng. Res. Des., **73**(A7), pp. 810–816.
[5] Benbow, J. J., Jazayeri, S. H., and Bridgwater, J., 1991, "The Flow of Pastes Through Dies of Complicated Geometry," Powder Technol., **65**(1–3), pp. 393–401.
[6] Davy, C. A., Bolton, M. D., and Fleck, N. A., 2004, "The Shearing Behaviour of a Sugar Aggregate," Acta Mater., **52**(12), pp. 3587–3601.
[7] Grimwood, C., 2005, *Filtering Centrifuges*, Elsevier, New York, Chap. 7.
[8] Werner, E., 1966, *Zuckertechniker-Taschenbuch*, Bartens, Berlin-Nikolassee, Germany.
[9] Drucker, D. C., and Prager, W., 1952, "Soil Mechanics and Plastic Analysis or Limit Design," Q. Appl. Math., **10**(2), pp. 157–165.
[10] Lade, P. V., and Duncan, J. M., 1975, "Elastoplastic Stress-Strain Theory for Cohesionless Soil," J. Geotech. Engrg. Div., **104**(1), pp. 139–141.
[11] Makarytchev, S. V., Xue, E., Langrish, T. A. G., and Prince, R. G. H., 1997, "On Modelling Fluid Flow Over a Rotating Conical Surface," Chem. Eng. Sci., **52**(6), pp. 1055–1057.
[12] MathWorks Inc., 2008, MATLAB 7.6.0.324 (r2008a), Natick, MA.
[13] Soltani, F., and Yilmazer, U., 1998, "Slip Velocity and Slip Layer Thickness in Flow of Concentrated Suspensions," J. Appl. Polym. Sci., **70**(3), pp. 515–522.